Editors' Suggestion

Designing an All-Carbon Membrane for Water Desalination

David Tománek[1,*] and Andrii Kyrylchuk[1,2]

[1] *Physics and Astronomy Department, Michigan State University, East Lansing, Michigan 48824-2320, USA*
[2] *Institute of Organic Chemistry, National Academy of Sciences of Ukraine, Murmanska Street 5, 02660 Kyiv, Ukraine*

(Received 14 June 2019; published 26 August 2019)

We design an all-carbon membrane for the filtration and desalination of water. A unique layered assembly of carbon nanostructures including graphite oxide (GO), buckypaper consisting of carbon nanotubes, and a strong carbon fabric provides high mechanical strength and thermal stability, resilience to harsh chemical cleaning agents, and electrical conductivity, thus addressing major shortcomings of commercial reverse osmosis membranes. We use *ab initio* density-functional-theory calculations to obtain atomic-level insight into the permeation of water molecules in between GO layers and across in-layer vacancy defects. Our calculations elucidate the reason for selective rejection of solvated Na^+ ions in an optimized GO membrane that is structurally stabilized in a sandwich arrangement in between layers of buckypaper, which are protected on both sides by strong carbon fabric layers.

DOI: 10.1103/PhysRevApplied.12.024054

I. INTRODUCTION

Availability of potable water is one of the most pressing needs of humankind [1]. Even though water is plentiful on Earth, most of it is not suited for human consumption and must be treated beforehand [1,2]. The key to processing contaminated or brine water is filtration. Micro- and nanoporous carbon has been used successfully for filtration due to its small pore size and large surface area, combined with its high chemical, thermal, and mechanical stability, as well as low cost [3,4]. Also salty seawater can be made potable using, among others, ultrafine membranes. We focus here on desalination based on reverse osmosis (RO) [5], which is more challenging than filtration due to the difficulty of separating solvated ions from water on the molecular level. State-of-the-art nanoporous membranes for water desalination achieve selective rejection of specific ions, typically utilizing polymers such as polysulfone. Such membranes do not operate well at high temperatures approaching that of boiling water, pressures of several hundred bar, and show limited resilience to chemicals used for cleaning of biofouling debris [6]. Carbon nanostructures have been considered in search of suitable alternatives, but they were found to be rather brittle and unsuited for membrane applications [7]. There have been calls for atomic-level theoretical investigations [1] and for a paradigm shift [1,8] to achieve serious progress in water desalination.

Here, we present a design of an all-carbon membrane for the filtration and desalination of water that should not suffer from previously reported materials limitations. The outermost layer of the proposed sandwich structure of the membrane would be a strong, yet flexible fabric of carbon fibers or carbon nanotubes (CNTs), capable of withstanding extremely high pressures used in the RO process. The innermost layer, which should separate water molecules from solvated ions including Na^+, would consist of layered, highly oriented graphite oxide (GO). This core layer would be sandwiched in between layers of buckypaper consisting of CNTs, which would also provide cushioning against the outermost layers. Using different polymorphs of graphitic carbon as membrane components should provide superior thermal and mechanical stability as well as resilience to harsh chemicals used to clean off biofouling debris. To investigate the viability of our concept, we use *ab initio* density-functional-theory calculations to obtain atomic-level insight into the permeation of water molecules in between GO layers and across in-layer vacancy defects. Our results elucidate the reason for the reported selective rejection of solvated Na^+ ions in an optimized GO membrane.

II. STRUCTURE AND FUNCTIONALITY OF THE PROPOSED ALL-CARBON MEMBRANE

A schematic view of the proposed all-carbon membrane, along with a likely trajectory of a water molecule permeating the membrane, is presented in Fig. 1(a). In the following, we first discuss the properties of the outermost

*tomanek@pa.msu.edu

 © 2019 American Physical Society

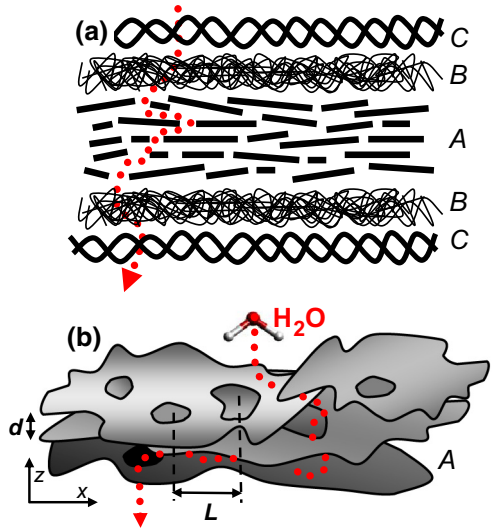

FIG. 1. Layered structure of the proposed all-carbon membrane suitable for water filtration and desalination. (a) Schematic side view of the membrane design. Core layer *A*, consisting of highly oriented GO, is sandwiched in between layers *B* of buckypaper and finally in between layers *C* of strong carbon fabric. (b) Detailed schematic view of the defective GO layers in the core *A* of the membrane, characterized by the interlayer distance *d* and the typical separation *L* between in-layer pores. Schematic route of a H_2O molecule across the membrane is indicated by the red dotted line.

layers *B* and *C* of the membrane, which are well known in the carbon community.

A. Outermost layers of bucky paper and carbon fabric

The two outermost layers *B* and *C* of the membrane in Fig. 1(a) consist of quasi-one-dimensional (1D) graphitic carbon nanostructures including CNTs and carbon fibers. Both benefit from the extraordinary properties of graphite or monolayer graphene (MLG), including its flexibility, in-plane tensile strength 100 times that of steel, melting temperature close to 4000 K, and resilience to harsh cleaning chemicals containing chlorine [9].

The buckypaper layer *B* consists of entangled single-wall CNTs with diameters of 1–2 nm, with its structure resembling a scouring pad [9–11]. The typical pore size, representing the internanotube spacing, ranges between 20 and 50 nm. Buckypaper does not impede the passage of water molecules or ions, but blocks larger debris [11,12]. The main purpose of layer *B* is to contain the layered, but brittle GO with typical flake sizes exceeding 1 μm in the core layer *A*.

The outermost carbon fabric layer *C* plays its most important role in structurally supporting and containing material in layers *A* and *B*. The pore size in layer *C* typically exceeds 1 μm and does not really matter as long as it contains the buckypaper layer. Since the pore sizes exceed those of buckypaper, this layer also does not impede passage of water molecules or ions. The strength and flexibility of the carbon fabric, which also protects the membrane from stone impact, is provided by CNTs, which can be harvested, spun into yarns [13], and woven into a fabric [14]. The presence of CNTs has been shown to reduce biofouling of membranes [15]. Since layers *B* and *C* are electrically conductive, applying a voltage may further assist in rejecting ions [16–18].

B. Layered GO

Key to the selective rejection of ions is the core layer *A* of the membrane consisting of GO. The structure of GO consists of MLG layers that have been chemically functionalized by epoxy-O and OH groups [19]. A simplified schematic image of a realistic GO structure is presented in Fig. 1(b). Unlike hydrophobic graphite and MLG, GO is hydrophilic and requires water for stabilization. In comparison to graphite, GO also has a lower biofouling tendency [20].

The two commonly used approaches to synthesize GO are the Hummer [21] and the Brodie [22] process. Both techniques yield an ordered material containing a substantial fraction of in-layer pores, seen in Fig. 1(b). For a long time, GO has been considered a viable material to form membranes, especially suitable for water desalination based on RO [19]. GO has been found to be very useful for the filtration and purification of water [23] and other substances, which have to cross many pores in many layers. GO membranes have come back into the focus of research due to progress in this direction. Because of its rather small grain size, as-produced GO is typically regarded as a powder. Related multilayer graphene oxide (MLGO), a new term coined for layered GO with large grains, has indeed proven useful for water purification and desalination [24]. A significant improvement of the nanofiltration capability of GO has been achieved by shear alignment [25]. We believe that homogenization of the GO sample by ball milling followed by shear alignment may optimize the performance of GO for water desalination.

Obviously, controlling the microscopic structure and layer alignment in GO and understanding the flow mechanism of water molecules in between layers of graphite [26] and GO [27,28] are crucial for further progress. Molecular dynamics simulations with model potentials [29,30] and neutron diffraction studies [29,31] have provided initial insight into the system. Still, atomic-scale information about the mechanism of water permeation and selective ion rejection by GO membranes is either absent or extremely limited.

C. Known facts about the permeation of H_2O molecules and salt ions in GO

The presence of in-layer pores in the layered structure of GO is a necessary prerequisite for water permeation

since no atoms could penetrate through the atomic lattice of an ideal membrane consisting of infinitely large, defect-free layers. We distinguish in-layer pores, consisting of extended vacancies and defects in a layered structure, from slit pores associated with the interlayer region that can accommodate external atoms and molecules. To allow water to permeate, pore sizes in the membrane must exceed the van der Waals diameter $d_{vdW}(H_2O) = 2.8$ Å of a H_2O molecule [32]. The key challenge is to allow only water and not salt ions to pass through the membrane by limiting the size and chemical termination of in-layer pores.

Description of ion transport across in-layer pores in GO must necessarily consider the fact that ions are hydrated and that the ionic hydration shell may change during the passage. It would therefore be misleading to compare the observed bare radii of salt ions [33] $r(Na^+) = 1.17$ Å, $r(K^+) = 1.49$ Å, and $r(Cl^-) = 1.64$ Å to the van der Waals radius $r(H_2O) = 1.4$ Å of a water molecule [32].

In an aqueous environment, all ions are surrounded by water molecules, which form a tightly bound hydration shell. Neutron diffraction studies [34] and DFT calculations [35] agree on the hydration shell radii that are slightly larger than the ion-oxygen distances $d(Na^+\text{-}O) =$ 2.3–2.4 Å, $d(K^+\text{-}O) =$ 2.7–2.8 Å, and $d(Cl^-\text{-}O) = 3.2$ Å. Unlike the cations, hydrated Cl^- ions form hydrogen-bonded bridges with water molecules [34]. The hydration shell of Na^+ and K^+ cations contains about six water molecules, while that of larger Cl^- anions contains about seven water molecules. The values of the sequential detachment energies of water molecules from the hydration shells of many ions are now well established [36]. For the ions of interest here, the detachment of all water molecules requires $E_{hyd}(Na^+) = 4.03$ eV, $E_{hyd}(K^+) = 3.46$ eV, and $E_{hyd}(Cl^-) = 3.27$ eV. These hydration energy values are significantly higher than the hydration energy of a water molecule [37] $E_{hyd}(H_2O) =$ 0.43 eV and have to be considered seriously in any desalination study.

Steric and energetic considerations suggest that with their largest hydration shell, Cl^- anions should pass with much less ease than the Na^+ and K^+ cations across a membrane containing nanopores. This expectation has been confirmed by the experimental finding [38] that K^+ and Na^+ behave in a similar way and that K^+ ions pass 100 times faster than Cl^- ions through a membrane. With their even larger hydration shells, divalent cations Ca^{++} and Mg^{++} have been observed to pass still more slowly than monovalent cations [38]. Therefore, we focus on the selective passage of water molecules and monovalent cations in this study.

Passage of ions through a membrane may be suppressed by limiting the pore size to that of the ionic hydration shell, with 6 Å for hydrated Na^+ representing a minimum value [35,39]. The major challenge in the desalination field is production of membranes with a very narrow range of pore sizes between 0.3 and 0.8 nm that enable passage of water, but not of hydrated ions.

In this study, we combine reported observations with original atomic-scale calculation results that should elucidate the permeation of water and specific rejection of ions in a GO membrane, which have eluded a consistent microscopic description so far.

D. Cleaning of biofouled all-carbon membrane

Biofouling of membranes can never be prevented and poses a significant problem in the RO process [6,20,40,41]. Conventional cleaning agents, which contain chlorine, not only remove biofouling agents, but also attack currently used polymer membranes, limiting their useful lifetime. One major benefit of an all-carbon membrane is the known resilience of carbon materials to cleaning agents containing chlorine and to other chemicals.

Stability of carbon membrane materials under temperatures well beyond 1000 °C suggests an unconventional alternative to chemical cleaning. For the purpose of cleaning, an all-carbon membrane could be separated from its holder, suspended in an oxygen-free nitrogen atmosphere, and heated resistively to high temperatures, when all biofouling deposits would decompose. The most stable product of the decomposition process should be nonspecific carbon nanostructures, which should provide additional structural reinforcement to the membrane material and potentially improve its performance without clogging it.

III. COMPUTATIONAL APPROACH

Our computational approach to study liquid water and Na^+ ions interacting with chemically functionalized, defective graphite and graphite oxide is based on *ab initio* density-functional theory (DFT) as implemented in the SIESTA [42] and VASP [43,44] codes. While computationally rather demanding, DFT calculations are free of adjustable parameters and provide bias-free predictions for molecular and solid systems. In this, our approach differs from parameterized force fields that are computationally faster, but offer limited transferability among different systems. We describe the effect of electron exchange and correlation using the nonlocal Perdew-Burke-Ernzerhof (PBE) [45] functional and compared selected results to those based on the local density approximation (LDA) [46,47]. The DFT PBE total energy functional has been used extensively to provide an unbiased description of water and its interaction with solids [26,48]. We use periodic boundary conditions throughout the study. Our SIESTA calculations use norm-conserving Troullier-Martins pseudopotentials [49], a double-ζ basis including polarization orbitals, and a mesh cutoff energy of 180 Ry to determine the self-consistent charge density, which provides us with a precision in total energy of $\lesssim 2$ meV/atom. The VASP calculations are performed using the projector augmented

wave (PAW) method [44] and 400 eV as the energy cutoff. The reciprocal space is sampled by a uniform k-point grid [50], as noted specifically. Systems with very large unit cells are represented by the Γ point only. Geometries are optimized using the conjugate gradient (CG) method [51], until none of the residual Hellmann-Feynman forces exceeds 10^{-2} eV/Å. Equilibrium structures and energies based on SIESTA are checked against values based on the VASP code. Microcanonical (NVE) and canonical (NVT) molecular dynamics (MD) calculations are performed using short 0.3-fs time steps, which are sufficiently short to guarantee energy conservation in microcanonical ensembles.

To represent the effect of pressure on the permeation of water and Na^+ ions, we modify the SIESTA source code to subject selected atoms to a constant force. To preserve interatomic distances and obtain a constant acceleration within a group of selected atoms, we subject each atom in the group to the force $\mathbf{F} = \mathbf{F}_0 \times m_a$, where m_a is the atomic mass in a.m.u. These driving forces, which typically amount to $|\mathbf{F}_0| \lesssim 2.5 \times 10^{-2}$ eV/Å, induce water flow along and across defective graphene and graphite oxide layers in our MD simulations.

IV. RESULTS

All our results reported in the following are based on *ab initio* total energy calculations and corresponding MD simulations. We use DFT to obtain static equilibrium structures including their energies and DFT-based MD simulations to describe the evolution of a system in time. Such numerical simulations are often referred to as computational experiments as they produce vast quantities of data, which need to be further analyzed. Both in real and computational experiments, error bars represent the uncertainty in the reported values. In computer simulations, error bars may be obtained from ensemble averages or estimated based on finite-size fluctuations in finite-time MD simulations.

A. Properties of liquid water

Whereas isolated H_2O molecules are well understood, correct description of liquid water has remained a challenging problem for decades [52]. Very many energy functionals have been developed to describe the delicate interplay among the strong and weak forces that determine the behavior of liquid water, but none has been able to satisfactorily reproduce all aspects of its behavior and interaction with solids in an unbiased manner. In spite of their relatively high requirement on computational resources, we use here *ab initio* DFT calculations to provide an unbiased description of water interacting with carbon-based membranes.

Our calculated hydration energy of a water molecule $E_{\mathrm{hyd,theo}}(H_2O) = 0.408$ eV agrees well with the observed value [37] $E_{\mathrm{hyd,expt}}(H_2O) = 0.430$ eV. The calculated gravimetric density of water $\rho_{\mathrm{theo}}(H_2O) = 0.9$ g/cm^3 agrees with previously reported DFT-PBE values [52–54] of 0.81–0.87 g/cm^3, but underestimates the observed value at room temperature [55] $\rho_{\mathrm{expt}}(H_2O) = 1.0$ g/cm^3.

To obtain insight into the dynamics of liquid water, we first consider its viscous behavior. To do so, we use the Einstein-Smoluchowsky equation, which relates the self-diffusion coefficient D of a Brownian particle in a $\tilde{d}$-dimensional space to its trajectory $\mathbf{r}(t)$ by

$$\langle |\mathbf{r}(t) - \mathbf{r}(0)|^2 \rangle = 2\tilde{d}Dt. \quad (1)$$

The dimensionality of bulk water in this equation is $\tilde{d} = 3$. We perform a limited-size MD simulation of 30 H_2O molecules per unit cell and trace the positions of water molecules by their center of mass as a function of time. Our simulation results shown in Fig. 3(e) suggest $D_{\mathrm{theo}} = (1.0 \pm 0.8) \times 10^{-5}$ cm^2/s for the self-diffusion coefficient. In spite of the large uncertainty caused by limited simulation time and the significant finite-size fluctuations, the estimated value of D is somewhat lower than the observed value [56] $D_{\mathrm{expt}} = 2.3 \times 10^{-5}$ cm^2/s $= 2.3 \times 10^{-9}$ m^2/s in bulk liquid H_2O at 25 °C. The fact that DFT PBE MD simulations typically underestimate the value of D, with results ranging from 0.1×10^{-5} to 0.6×10^{-5} cm^2/s, has been reported previously [52,57]. Also, the higher initial slope of the mean-square displacement in our MD simulation, caused by initial ballistic motion of H_2O, agrees with previously reported behavior [58].

B. Representation of graphite oxide

Whereas the honeycomb lattice of graphene, with atoms separated by 1.42 Å, has been known for a long time [60], its oxidized counterpart—GO—is not as clearly defined and contains covalently attached epoxy-O and OH groups that may vary in their spatial distribution. GO may contain isolated nonoxidized graphitic regions amounting to less than 15% by area [61]. The most commonly used representation of fully oxidized GO is the Lerf-Klinowski model [31,59] shown in Fig. 2.

C. Interaction of H_2O molecules with graphite and GO layers

As a water molecule adsorbs on graphene or graphite, it gains the adsorption energy $E_{\mathrm{ad,theo}}(H_2O/\mathrm{MLG}) = 0.14$ eV according to our DFT PBE results. This is similar to the observed value [62] $E_{\mathrm{ad,expt}}(H_2O/\mathrm{MLG}) \lesssim 0.20$ eV, which is likely overestimated [48]. The interaction energy of a two-dimensional (2D) water monolayer with graphene, amounting to 0.02 eV per H_2O molecule, is 1 order of magnitude smaller. Adsorption of initially free water molecules and their subsequent condensation to a 2D monolayer on graphene provides a

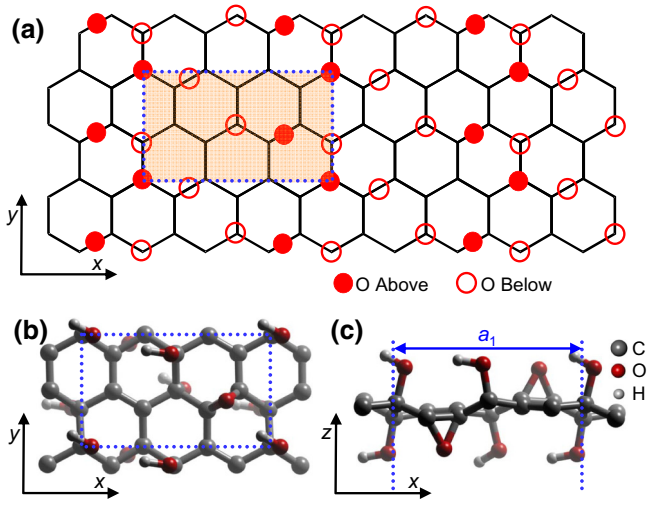

FIG. 2. Monolayer of graphite oxide in the Lerf-Klinowski model [59] according to Ref. [31]. (a) Schematic representation in top view, indicating the position of epoxy-O in bridge sites and OH groups in on-top sites above and below carbon atoms in the graphene monolayer. Ball-and-stick models of optimized GO in (b) top view and (c) side view, indicating a substantial degree of wrinkling. The primitive unit cell is delimited by the dotted blue line and indicated by shading in (a).

larger energy gain of 0.39 eV per water molecule. All these values are significantly lower than the hydration energy $E_{\mathrm{hyd,theo}}(H_2O) = 0.408$ eV of a water molecule in water. Energetic preference of H_2O to be surrounded by other water molecules rather than graphitic carbon makes graphene and graphite hydrophobic.

We could not confirm the reported formation of 2D square ice on a graphene monolayer [63], which has been questioned subsequently [64], based on our total energy results, which suggest energy differences of only a few meV/molecule due to molecular ordering. Such small energy differences are consistent with previously reported theoretical results [65], indicating easy sliding of H_2O molecules in between graphene layers.

We find the adsorption energy of a water molecule on GO to be significantly higher than on graphene and graphite. Depending on the adsorption site, typical values range near $E_{\mathrm{ad,theo}}(H_2O/GO) = 0.73$ eV, exceeding the hydration energy of H_2O significantly. This indicates that water molecules prefer energetically to be near GO rather than surrounded by water only, making GO hydrophilic on the molecular level. Our findings for isolated water molecules are only indicators that should not be taken as substitutes for the behavior of liquid water.

In a more realistic description, we consider the permeation of water in a carbon-based layered system, namely, GO or graphite, using the periodic geometry shown in Fig. 3(a). A snapshot of water molecules arranged in between GO layers is shown in Fig. 3(b). Per unit cell with in-layer area A and height d, the water permeation energy ΔE_{perm} associated with the transfer of m water molecules from liquid water to the interlayer region can be estimated by obtaining the energy difference between the water-permeated system, bulk water, and the bulk dry carbon-based system. The carbon-based system is hydrophobic if $\Delta E_{\mathrm{perm}} > 0$ and hydrophilic if $\Delta E_{\mathrm{perm}} < 0$, indicating that water molecules prefer energetically the interlayer space in the carbon-based system to bulk water. Beyond a critical content of water, amounting to many H_2O molecules per unit cell and corresponding to several layers of water in the interlayer space, ΔE_{perm} should approach a constant value describing noninteracting GO layers solved in bulk water.

We found the energy balance in the calculation of ΔE_{perm} to depend delicately on the arrangement of water molecules in the interlayer region. To compensate for this uncertainty to some degree, we first calculated $\Delta\tilde{E}_{\mathrm{perm}}$ not with respect to bulk H_2O, but rather free-standing layers of H_2O in exactly the same configuration as in the interlayer space of the carbon-based layered system. Then, we determine $\Delta E_{\mathrm{perm}} = \Delta\tilde{E}_{\mathrm{perm}} + 2\gamma A$, where A is the area of the unit cell in the plane of the layers and γ is the surface tension of liquid water, which in turn depends on its surface structure in calculations. We use $A = 41.9$ Å^2 for optimized graphene with a 16-atom supercell, $A = 43.1$ Å^2 for GO terminated with O-epoxy groups, $A = 41.0$ Å^2 for GO terminated with OH groups, and $A = 32.3$ Å^2 for the Lerf-Klinowski model [31,59] of GO shown in Fig. 2. Based on the density distribution of water molecules and structural snapshots such as Fig. 3(b), we find that distinguishable water layers contain typically five molecules per unit cell in our calculation, which helps in correlating the number m of water molecules with the number of water layers.

Theoretical estimates of γ range from 6.6×10^{-2} J/m^2 based on DFT PBE MD simulations [66] to the estimated value $\gamma \lesssim 65.9 \times 10^{-2}$ J/m^2 based on our DFT PBE structure optimization studies for different geometries. The observed value [67] $\gamma = 7.3 \times 10^{-2}$ J/m^2 at 20 °C falls into this value range and so does the value $\gamma = 14.0 \times 10^{-2}$ J/m^2 that we select to estimate the water permeation energy.

Our results for ΔE_{perm} as a function of the number m of the water molecules per unit cell are presented in Fig. 3(c). Based on the sign of ΔE_{perm}, we conclude that the H_2O/GO system is hydrophilic and the H_2O/graphite system is hydrophobic in agreement with observation. The simulation data points are subject to variations caused by the amorphous structure of liquid water that is continuously changing. Among the GO systems, we find GO-OH to be most and GO-epoxy to be least hydrophilic, with the Lerf-Klinowski model containing both OH- and O-epoxy groups to lie in between. There even appears to be preference for about two water layers in GO according to the Lerf-Klinowski model, in agreement

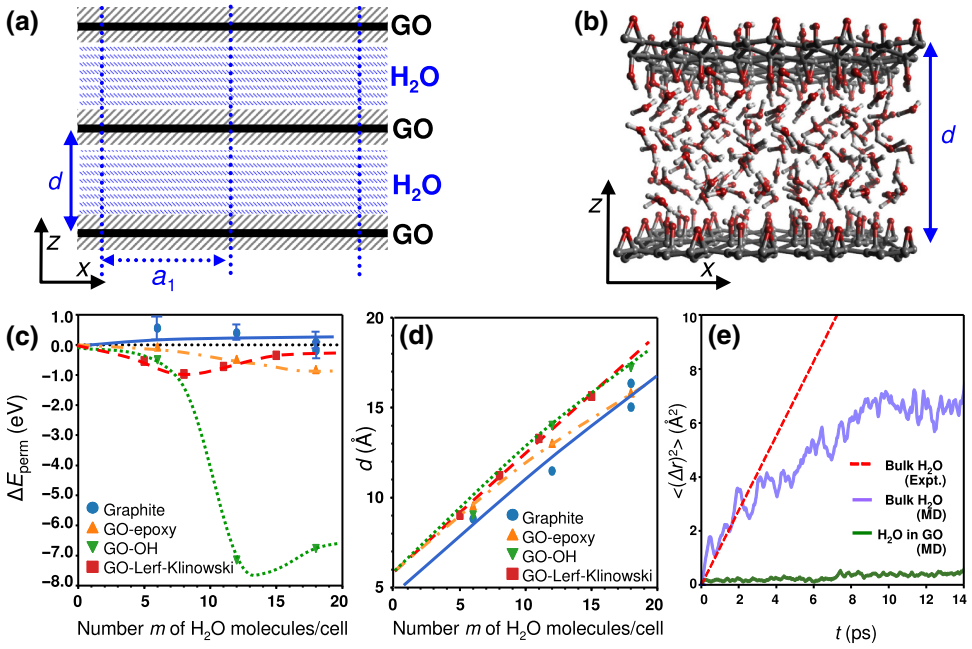

FIG. 3. Permeation of water in GO. (a) Schematic side view of the periodic structure of GO layers separated by water. The GO unit cell of width a_1 and height d is the same as in Fig. 2. (b) Snapshot of the arrangement of H_2O molecules in a 14.72 Å wide segment of GO with the interlayer separation $d = 12.85$ Å. (c) Energy gain ΔE associated with the presence of m water molecules in the interlayer region. (d) Optimized height d of unit cells containing m water molecules. (e) Comparison of the mean-square displacement of H_2O molecules in bulk water and in the constrained space in between GO layers shown in panel (b). Extrapolation based on experimental data in bulk water is shown for comparison by the red dashed line.

with observation [27], and about three water layers in GO-OH, probably due to the favorable registry of water molecules with the functionalized carbon layers. We find that energy changes in the system are largest during the initial permeation of water in between the layers, eventually reaching a saturation value. With $m \approx 5$ water molecules per water layer in the unit cell, we may consider systems with $m \gtrsim 15$ to represent a fully hydrated system.

We present the optimized interlayer distance d as a function of water filling in Fig. 3(d). The increase of d due to water permeation, starting from $d \approx 6$ Å in dry GO, is called swelling. In a RO system containing a GO-based membrane, swelling is limited by the pressure difference between the two sides of the membrane and by interlayer bonds that hold a defective GO membrane together.

In agreement with previously reported theoretical [35] and experimental data [39], we find the optimum size of the Na^+ hydration shell to be close to 6 Å. Since the interlayer distance d in GO permeated with water is significantly larger, hydrated Na^+ ions are likely to permeate in and propagate within the interlayer region in a similar way as bulk water.

To learn more about water flow within slit pores in GO, we first study the diffusion of a water molecule along the armchair direction in the GO layer, aligned with the y axis in Fig. 2(a). To obtain bias-free energy information along the diffusion path, we perform a set of global optimizations while constraining the y coordinate of the O atom of the water molecule and allowing this atom to move only within the x-z plane normal to GO layers. The energy change ΔE along the trajectory is shown in Fig. 4(a) and a superposition of corresponding snapshots of the molecule is shown in Fig. 4(b). Because of the activation barriers for water propagation along the slit pore, the self-diffusion coefficient is reduced significantly with respect to the bulk water value, as seen in Fig. 3(e). Our estimated value of

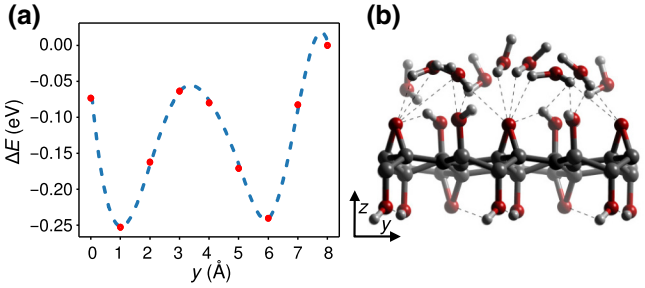

FIG. 4. Diffusion of a water molecule confined in the x-z plane normal to GO layers along the GO layers within a slit pore in between the layers. (a) Energy change ΔE as the water molecule diffuses along the armchair direction y of GO. (b) Snapshots of water molecule configurations along the diffusion path, corresponding to the simulation data points in (a), with hydrogen bonds indicated by the dashed lines. The line connecting the simulation data points in (a) is a guide to the eye.

the self-diffusion coefficient of water in GO is $D_{\text{theo}} = 8 \times 10^{-7}$ cm^2/s. The significant reduction in the calculated value of D from bulk water to water in GO is consistent with the observation [68,69] that D is several times lower for water under both hydrophilic and hydrophobic confinement than in bulk water.

We should note that self-diffusion under ambient conditions is unrelated to the pressure-driven propagation of water molecules along the slit pores. Still, the related reduction of the mobility of water molecules adjacent to the GO layers is another validation of the assumptions used in the Hagen-Poisseuille description of pressure-driven flow of liquids through pores and pipes [70].

To study pressure-induced water permeation along slit pores, we fill the space in-between GO layers, defined in Fig. 3(a), partly with water. To observe the formation of a meniscus and the dynamics of the propagating water front, we separate segments completely filled with water by water-free segments. All atoms in the water molecules are subject to the force $F = F_0 \times m_a$, where m_a is the atomic mass and $F_0 = 6.25 \times 10^{-3}$ eV/Å, acting along the slit pores. We perform MD simulations of the evolution of the system lasting about 1 ps in total and follow the acceleration of the water molecules. Unlike in unconstrained bulk water, water molecules in between GO layers are slowed down by a drag force $F_{0,\text{drag}}$, acting on both H and O atoms and originating in the interaction between the moving molecules and the GO layers. Videos of the propagation of water molecules along the slit pores are presented in Sec. A of the Supplemental Material (SM) [71].

For one monolayer of water, the distance between GO layers is fixed at $d = 9.03$ Å and the drag force is found to be $F_{0,\text{drag}} = 5.0 \times 10^{-3}$ eV/Å, almost 80% of the driving force. For three monolayers of water in between GO layers separated by $d = 12.9$ Å, the drag force drops to $F_{0,\text{drag}} = 2.5 \times 10^{-3}$ eV/Å, about half the value for a water monolayer. For the sake of comparison, we also consider a monolayer of water contained in between graphene layers separated by $d = 6.57$ Å. Applying the same accelerating force as in GO, we find a drag force of only $F_{0,\text{drag}} = 0.3 \times 10^{-3}$ eV/Å, 1 order of magnitude smaller than for water in GO.

We interpret these results in the following way. Whereas the water layers next to GO are nearly immobile, other water molecules in the middle of the slit pore are not affected much by the constraints. This is different in (hydrophobic) graphite, where none of the water layers would be slowed down by contact with graphene.

D. Interaction of H_2O molecules with defects in graphite and GO

As mentioned above, the presence of defects and pores in graphite and GO is essential for the permeation of water through corresponding membranes. The two characteristic edges of extended in-layer pores of interest here are the armchair and zigzag edge, obtained by cleaving graphene along the corresponding direction. Under ambient conditions, graphitic edges are not bare, but chemically terminated. The interaction of water molecules with these edges depends to a significant degree on the termination with hydrogen, hydroxy, and oxygen groups. The presence of these groups in the edge termination of GO has been established [72] and their functionality should be similar to that in a graphene edge. The optimum geometries of water molecules interacting with graphitic edges is depicted in Fig. 5 and our numerical results for the adsorption energies of water molecules are summarized in Table I.

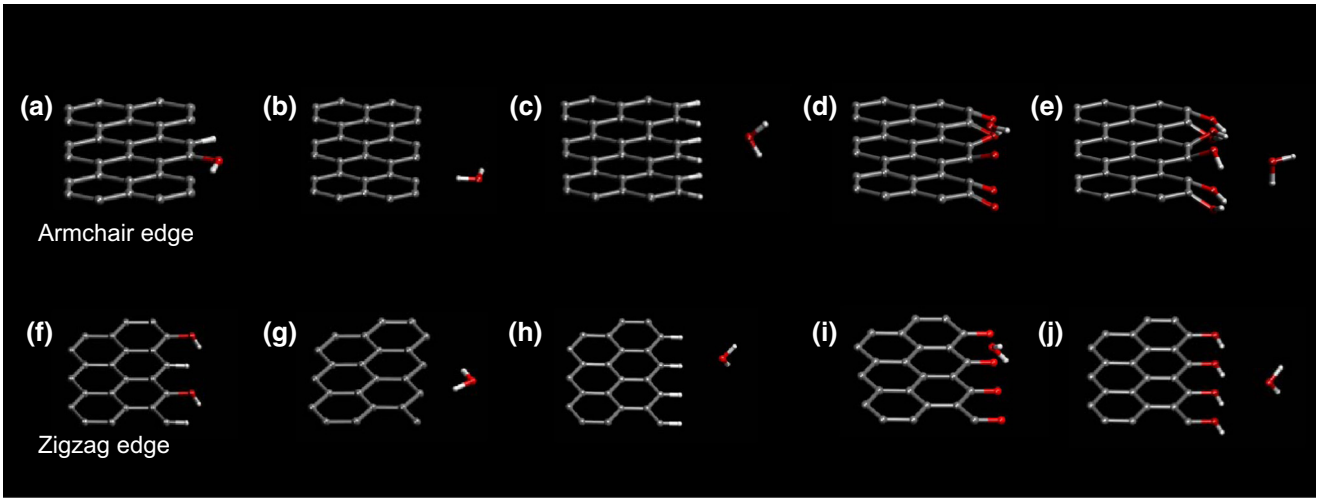

FIG. 5. Optimum geometry of a H_2O molecule interacting with (a)–(e) armchair and (f)–(i) zigzag edges of a graphene monolayer. Bare edges support both (a),(f) dissociative chemisorption and (b),(g) physisorption. Only physisorption occurs on (c),(h) H-terminated; (d),(i) O-terminated; and (e),(j) OH-terminated edges.

TABLE I. Adsorption energy E_{ad} of an isolated H_2O molecule at graphene edges. Reported results are for bare as well as H-, O-, and OH-terminated armchair and zigzag edges.

Edge termination	E_{ad} (armchair)	E_{ad} (zigzag)
Bare ($H_2O \rightarrow H_{ad} + OH$)	−4.75 eV	−5.27 eV
Bare	−0.02 eV	−0.21 eV
H-terminated	−0.10 eV	−0.03 eV
O-terminated	−0.14 eV	−0.10 eV
OH-terminated	−0.08 eV	−0.03 eV

Energetically most favorable for the water molecule near a bare graphene edge is dissociative adsorption, shown in Figs. 5(a) and 5(f), which splits H_2O and binds the resulting OH-radical and hydrogen to the edge covalently with a net energy gain of 4–6 eV according to Table I. The metastable physisorbed structures, shown in Figs. 5(b) and 5(g), are bound much more weakly according to Table I, similar to the adsorption on H-, O-, and OH-terminated edges. Among these, there is a small energetic preference for the functionalized armchair edges.

E. Representation of in-layer pores in graphite and GO

In our numerical study, we represent in-layer pores in GO by an infinite array of graphene nanoribbons with chemically functionalized armchair and zigzag edges and changing the in-layer separation width W. The structure of such pores is shown in Fig. 6.

F. Permeation of H_2O and ions through in-layer pores in GO

The key functionality of GO membranes in the desalination process is in allowing water molecules to pass through in-layer pores, while suppressing passage of hydrated salt ions such as Na^+. Since the interlayer distance in GO permeated with water is significantly larger than the size of hydrated Na^+ ions, we must consider the presence of both Na^+ ions and H_2O molecules in the interlayer region in GO. Then, the passage of hydrated Na^+ ions across in-layer pores needs to be investigated in the same fashion as that of water molecules.

Most important for the passage of molecules and ions through an in-layer pore is its geometry, including the edge termination. As mentioned before, the molecular sieving process is not affected by the layer geometry beyond the atomically close vicinity of the pore. Thus, we represent in-layer pores in defective GO layers by infinite arrays of graphene nanoribbons with armchair and zigzag edges, shown in Fig. 6, which are better defined and easier to treat computationally. We considered pores of different width W, defined by the separation of closest carbon atoms at pore edges, terminated with hydrogen, hydroxy, and oxygen groups [72].

Our results for the passage of isolated water molecules and hydrated Na^+ ions through different in-layer pores are presented in Fig. 7. Corresponding videos of permeating water molecules are presented in Sec. B of the SM and those of permeating hydrated ions in Secs. D and E of the SM [71]. To provide a realistic description of the activated process, we perform global optimization of the system while only fixing in-layer carbon atoms and the height h of the molecule or ion above the in-layer pore. As seen in Figs. 7(a) and 7(b), passage of both H_2O and Na^+ through most narrow pores with $W = 7$ Å is energetically activated, independent of edge geometry and termination. Activation-free passage is only possible through $W = 7$ Å pores with H-terminated armchair edges for H_2O and O-terminated armchair edges for Na^+. While passing an in-layer pore, water molecules lie preferentially in a plane normal to the carbon layer that passes through the pore.

According to Figs. 7(c) and 7(d), the activation barrier for water passage drops down to zero in wider pores with $W = 9$ Å, whereas the activation barrier for hydrated Na^+ ions remains substantial with the exception of O-terminated zigzag edges. As seen in the snapshots from the optimized trajectory in Figs. 7(c) and 7(f), Na^+ ions lose most of their hydration shell during the passage through the pore, which accounts for much of the energy cost. As expected, the energy difference $\Delta E(h)$ is symmetric around $h = 0$.

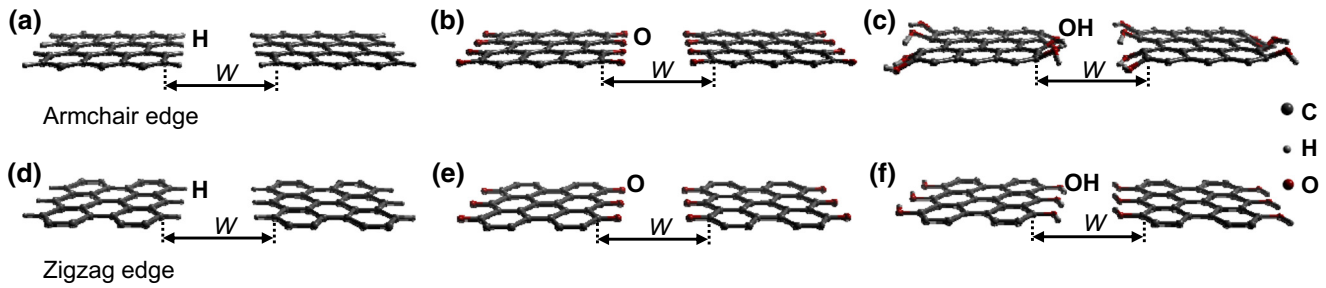

FIG. 6. Optimum geometry of an idealized in-layer pore formed by cleaving a graphene monolayer along the armchair or the zigzag direction. The (a)–(c) armchair and (d)–(f) zigzag edges may be chemically terminated by (a),(d) −H; (b),(e) −O; or (c),(f) −OH groups. The pore width W is defined by the separation of closest carbon atoms at opposing pore edges.

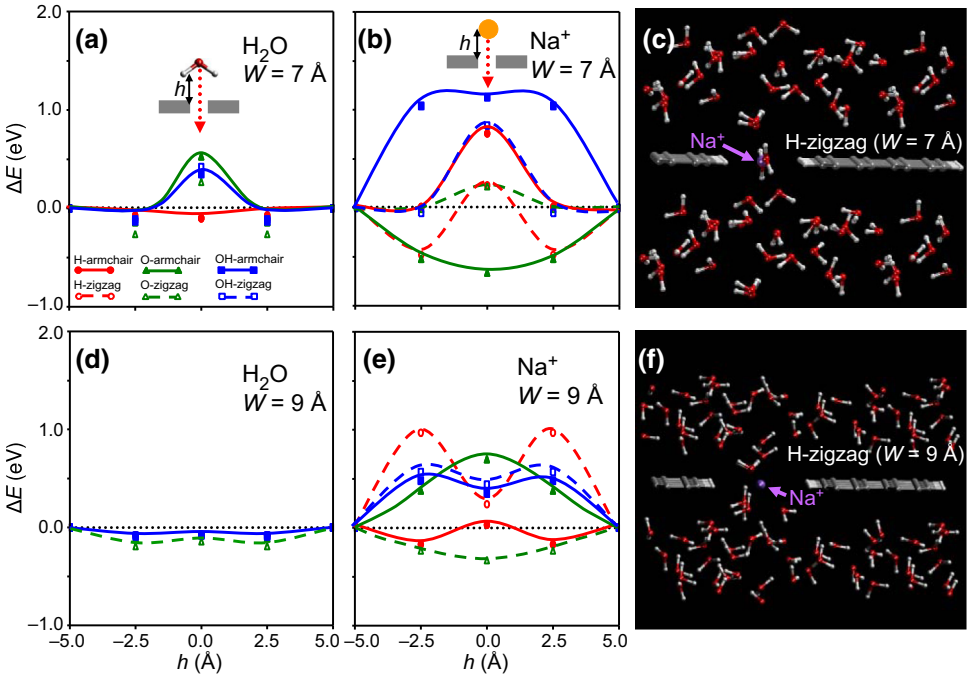

FIG. 7. Permeation of an isolated H_2O molecule and of hydrated Na^+ ions through in-layer pores with different pore widths W and different chemical terminations. h represents the vertical distance between the centroid of H_2O or the ion and the closest carbon layer. Lines connecting the simulation data points are guides to the eye.

Taking into the account the van der Waals radius of hydrogen [73] of 1.2 Å, the effective size of an in-layer armchair pore, shown in Fig. 6(a), is reduced significantly in the presence of terminating hydrogen atoms. Thus, terminating hydrogen reduces the effective opening of a $W =$ 7 Å wide pore to 4.6 Å and that of the even narrower $W = 5$ Å pore to merely 2.6 Å, less than the van der Waals diameter $d_{vdW}(H_2O) = 2.8$ Å of a H_2O molecule [32]. In the latter case, the passage of a single H_2O molecule requires local deformation of the pore at the energy cost $\Delta E = 1.1$ eV. Most favorable deformations at the pore edge will likely involve bending and not stretching or compression of C—H bonds, as indicated by observed IR frequencies in aromatic hydrocarbons, which suggest that bending a C_{ar}—H bond requires three times less energy than stretching this bond [74]. The same rule applies for other terminating groups as well. Therefore, in order to allow a water molecule subject to an external force to

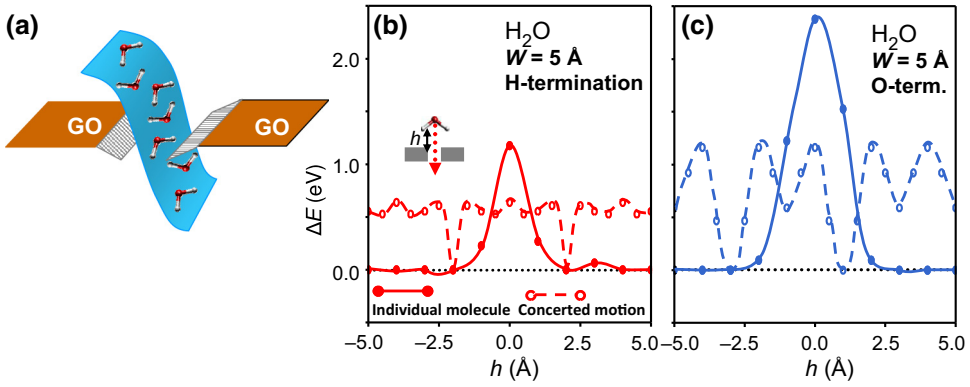

FIG. 8. (a) Schematic of the concerted motion of water molecules across a chemically terminated in-layer pore in GO. Calculated energy change ΔE per H_2O permeating either individually or in concerted manner through an in-layer pore of width $W = 5$ Å with (b) hydrogen-terminated and (c) oxygen-terminated armchair edges. h represents the vertical distance between the centroid of H_2O and the closest carbon layer. Concerted motion of molecules, indicated by the open symbols and the dashed lines, is compared to the passage of individual molecules, indicated by the solid symbols and the solid lines. Lines connecting the simulation data points are guides to the eye.

pass through an in-layer pore, the terminating atoms at the two sides of the pore preferably deflect in the same direction, as indicated in Fig. 8(a), in much the same way as a saloon door swings open when a drunk patron is thrown out.

In a process benefiting water, but not solved ions, energetically activated passage of H_2O molecules through narrow in-layer pores may be further promoted by concerted motion involving many molecules connected by hydrogen bonds as discussed in the following subsection.

G. Concerted motion of H_2O molecules through in-layer pores in GO

Understanding the passage of a single water molecule across the pore is of limited value in view of the fact that water molecules are connected in a network of hydrogen bonds. A more realistic scenario considers many water molecules passing through the in-layer pore at the same time, like a waterfall, depicted schematically in Fig. 8(a). Instead of one water molecule, we consider a 2D array of molecules confined in a plane normal to and containing the pore in GO. It is appealing to consider water molecules assisting each other energetically in the passage through an in-layer pore by preventing the relaxation of the terminating edges to the "closed" position, just as saloon patrons may keep the swinging door open for each other when entering. Our results, shown in Fig. 8(b) for a hydrogen-terminated and in Fig. 8(c) for an oxygen-terminated edge, indicate that the concerted motion of water molecules may indeed reduce the energy barrier for their passage from 1.1 to 0.6 eV in the case of hydrogen termination and from 2.3 to 1.3 eV for oxygen termination, almost to half the original value. Videos of the concerted motion of H_2O molecules across an in-layer pore are shown in Video 1 and in Sec. C of the SM.

H. Permeation of different ions through in-layer pores in GO

As mentioned above, both isolated and hydrated K^+ ions are significantly larger than Na^+ ions. Nevertheless, K^+ ions are known to be transported across protein membranes in preference to Na^+ ions [75,76]. Even though protein membranes are significantly more complex than in-layer pores in GO, the postulated reason for this behavior being the stronger hydration shell of Na^+ as compared to K^+ ions [77] applies in both cases.

We compare permeation of Na^+ and K^+ ions in water across hydrogen-terminated in-layer armchair pores in graphene with $W = 5$ Å and $W = 7$ Å. To simulate this process, we perform microcanonical MD simulations of the system that is initially equilibrated at $T = 300$ K. We monitor changes in the potential energy $\Delta E_{\rm pot}(t)$ of the system as a function of time. During the run, all water molecules and ions are subject to an external force characterized by $|\mathbf{F}_0| = 6.25 \times 10^{-3}$ eV/Å, applied normal to the graphene layers. No constraints are applied during the 0.6-ps-long simulations except for fixing all carbon atoms in their positions. The results of our single-trajectory simulations are presented in Fig. 9. We note that these results should only be considered illustrative of the process and that ensemble averages over many trajectories would be required for any quantitative conclusions.

As expected, the action of the external force gradually increases the total energy and, in view of the virial theorem, also the potential energy of the system. Geometries corresponding to relative minima in $\Delta E_{\rm pot}(t)$ graphs are to be considered more stable. We find it interesting that the point of ion penetration across the layer, defined by $h = 0$, is not prominent in any of the graphs. This indicates that the relative position of water molecules with respect to the pore plays as important role as that of the ions. In view of the uncertainty caused by the finite size and complex structure of the system, ions pass

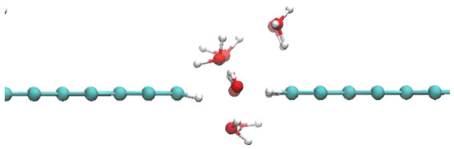

VIDEO 1. Concerted motion of water molecules permeating across an in-layer pore, represented by a pair of hydrogen-terminated armchair graphene nanoribbons separated by $W = 5$ Å.

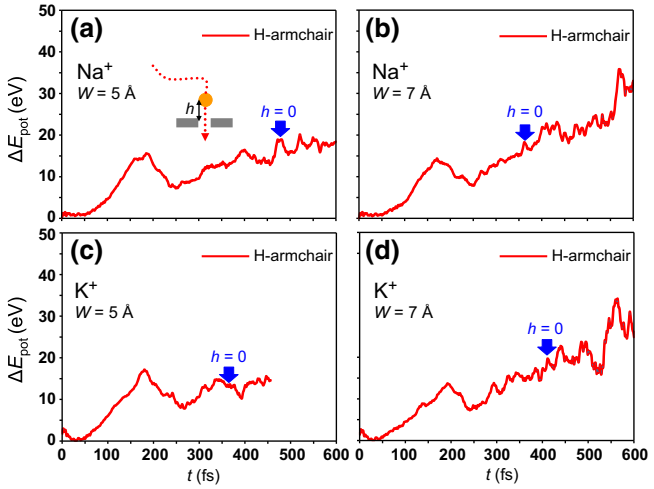

FIG. 9. Changes in the potential energy of the system $\Delta E_{\rm pot}$ as fully hydrated (a),(b) Na^+ and (c),(d) K^+ ions are driven by an applied force to pass through a hydrogen-terminated in-layer pore in graphene with armchair edges. Simulation results for pores of width $W = 5$ Å in (a),(c) are presented next to results for wider pores with $W = 7$ Å in (b),(d). Each unit cell contains one ion and 28 H_2O molecules. h represents the vertical distance between the ion and the closest carbon layer.

faster through wider pores than through narrower pores. We find substantial peaks in $\Delta E_{\mathrm{pot}}(t)$ at $t \lesssim 200$ fs in all trajectories and associate them with the energy cost to rearrange water molecules adjacent to the ions and the pore in order to enable the passage of the ion across the pore. With respect to this configuration prior to passage through the pore, the one corresponding to $h = 0$ may be either more stable, as in Fig. 9(c), or less stable, as in the other panels. Based on these preliminary results, we cannot find any conclusive evidence for preferential passage of Na^+ or K^+ ions through in-layer pores in graphene or GO.

V. DISCUSSION

The major objective of our study is to find whether GO is a viable material for water desalination [19] as postulated by many since the 1960s. To mitigate the brittle nature and related shortcomings of GO, we postulate a sandwich structure containing ultrastrong carbon nanotubes and graphitic carbon fabric in the outer layers enclosing the GO core layer. One of the key motivations for our study is the urgent call for a paradigm shift in the desalination membrane community, largely unaware of recent progress in ultrastrong carbon nanotubes, and the desire of the carbon nanotube community to locate a "killer application". Based on what has been known about each component of the system, and based on our microscopic *ab initio* calculations detailing atomic-scale processes occurring in the GO layer, we find the proposed all-carbon membrane well worth considering seriously for water desalination and encourage its experimental realization.

The proposed membrane design addresses the most urgent problems in water desalination, namely, selective salt rejection falling short of its objective [78] and irreversible biofouling. We identify structural parameters that should maximize salt rejection by GO without sacrificing water permeability. We believe that mechanical treatment of GO by ball milling and shear alignment may provide a uniform system well suited for its purpose. Graphitic carbon nanostructures forming the layers surrounding GO are now well established for their mechanical strength, flexibility, electrical and thermal conductivity, and resilience to extreme heat and to chemicals. Very important is the fact that all components of the all-carbon membrane are commercially available at very low cost.

Selective rejection of ions and reduction of its biofouling propensity may result from charging the conductive membrane possibly by a pulsed current [16]. Additional resistance against biofouling may be provided by continuously changing the morphology of the outermost layers of the proposed all-carbon membrane [79]. This should be possible, because individual components are graphitic structures that, under compression, may kink or wrinkle, but not uniformly shrink due to the high in-plane rigidity or graphene. Since RO membranes are not static objects, but rather vibrate under operating conditions, the membrane surface will continuously change its morphology and thus detach debris and biofouling agents [79].

Key to selective rejection of ions and permeation of water molecules is the morphology and chemical treatment of the central GO layer. The hydrophilic nature of GO can be regulated by modifying the density of OH terminating groups. The size and nature of in-layer pores, which we find critical for the desalination process, can initially be optimized during the ball-milling and shear alignment process. Membranes with fine pores are suitable for deionizing water, whereas coarse-pored membranes find their use in multistage RO systems or in decreasing the salinity of brines. Besides their smaller size compared to hydrated ions, water molecules benefit from their ability to pass through even very narrow pores by concerted motion with quite low activation barriers. Even 5-Å wide pores are still permeable while providing high salt rejection.

According to our results, 7-Å pores provide the best permeability ratio between H_2O and Na^+, whereas still wider 9-Å pores provide lower selectivity. The mechanical strength and flexibility of graphitic carbon allows adjusting the operating pressure, which should modify the pore size in order to adjust salt rejection and water flux as needed. Measuring and feeding these data continuously to a control system should allow on-the-fly tuning of operating pressure in response to changing feed water parameters [80]. Pores should open at higher and close at lower pressures, modifying the performance of the membrane. The range of operating parameters, with pressure being the most important of them, which optimize specific aspects of the RO membrane performance, can be studied in pilot plants and provided to the consumer by the manufacturer.

According to our simulations and common chemical intuition, the presence of OH groups is largely responsible for turning hydrophobic graphite into hydrophilic GO. As shown in our study, hydrophilic interlayer slit pores in GO attract ions and reduce their mobility, thus further decreasing permeation of salt in a similar way as in-layer pores do [30]. For this reason, increasing the number of OH groups at the expense of epoxy groups is highly desirable from the point of view of salt rejection.

As mentioned in the text, edges of in-layer pores are unlikely to remain bare and will acquire terminating groups under ambient conditions. We study three likely candidates for chemical termination, namely, H, epoxy-O, and OH groups, but do not observe significant differences from the viewpoint of water and salt permeation except a minor preference for hydrogen termination. Given a fixed in-layer pore width W, hydrogen termination hinders entering water molecules least due to its small size. Also, the activation barriers for the passage of Na^+ through H-terminated pores are not the highest. However, hydrogen-terminated pores provide the highest $\Delta E(H_2O)/$

$\Delta E(Na^+)$ ratio, which means that they maximize the permeability difference—the quantity we strive to increase. Hydrogen termination is also favored, because C-H groups interact only weakly with dissolved ions.

As we can infer from Fig. 7, Na^+ ions appear to be stabilized inside some O- and OH-terminated pores, resulting in a "negative barrier height." The reason for this behavior is the arrangement of O atoms in these pores, which provides an excellent coordination sphere for sodium cations, resembling the structure of the ion channel selectivity filter [75]. If the cation binding is too strong, the first cation that enters the pore will clog it. If the binding is weaker, small energetic preference for the in-pore site may promote cation passage by the adsorption-desorption mechanism. Unlike O- and OH-terminating groups, terminating hydrogens act mostly like a mechanical brush without the potential negative side effects.

VI. SUMMARY AND CONCLUSIONS

We design an all-carbon membrane for the purpose of filtering and desalinating water. The membrane contains graphite oxide sandwiched in between layers of buckypaper consisting of carbon nanotubes, and the entire structure is contained in between layers of strong carbon fabric from both sides. The structure combines high mechanical strength with thermal stability and resilience to harsh chemical cleaning agents with electrical conductivity, thus addressing major shortcomings of commercial RO membranes. We use *ab initio* DFT calculations to provide atomic-level insight into the permeation of water molecules in between GO layers and across in-layer vacancy defects. Our calculations elucidate optimum conditions for permeation of water and selective rejection of solvated Na^+ ions by the membrane. We anticipate that the viability of the designed structure will be confirmed experimentally in the near future.

ACKNOWLEDGMENTS

D.T. acknowledges financial support by the NSF/AFOSR EFRI 2-DARE Grant No. EFMA-1433459. A.K. acknowledges financial support by the Fulbright program. We thank Igor Baburin, Morinobu Endo, Katsumi Kaneko, Takeyuki Kawaguchi, James Linnemann, Dan Liu, Alexander Quandt, Gotthard Seifert, Alexandr Talyzin, Akihiko Tanioka, and Volodymyr Tarabara for valuable discussions. Computational resources are provided by the Michigan State University High Performance Computing Center.

Note added.—We have recently learned of a different all-carbon desalination membrane, which has demonstrated superior performance over current technology [81].

[1] Menachem Elimelech and William A. Phillip, The future of seawater desalination: Energy, technology, and the environment, Science **333**, 712 (2011).
[2] Jay R. Werber, Chinedum O. Osuji, and Menachem Elimelech, Materials for next-generation desalination and water purification membranes, Nat. Rev. Mater. **1**, 16018 (2016).
[3] Albert Boretti, Sarim Al-Zubaidy, Miroslava Vaclavikova, Mohammed Al-Abri, Stefania Castelletto, and Sergey Mikhalovsky, Outlook for graphene-based desalination membranes, npj Clean Water **1**, 5 (2018).
[4] Gongping Liu, Wanqin Jin, and Nanping Xu, Graphene-based membranes, Chem. Soc. Rev. **44**, 5016 (2015).
[5] Yoram Cohen, Raphael Semiat, and Anditya Rahardianto, A perspective on reverse osmosis water desalination: Quest for sustainability, AIChE J. **63**, 1771 (2017).
[6] David M. Warsinger, Sudip Chakraborty, Emily W. Tow, Megan H. Plumlee, Christopher Bellona, Savvina Loutatidou, Leila Karimi, Anne M. Mikelonis, Andrea Achilli, Abbas Ghassemi, Lokesh P. Padhye, Shane A. Snyder, Stefano Curcio, Chad D. Vecitis, Hassan A. Arafat, and John H. Lienhard, A review of polymeric membranes and processes for potable water reuse, Prog. Polym. Sci. **81**, 209 (2018).
[7] Pengzhan Sun, Kunlin Wang, and Hongwei Zhu, Recent developments in graphene-based membranes: Structure, mass-transport mechanism and potential applications, Adv. Mater. **28**, 2287 (2016).
[8] Muhammad Wakil Shahzad, Muhammad Burhan, Doskhan Ybyraiymkul, and Kim Choon Ng, Desalination processes' efficiency and future roadmap, Entropy **21**, 84 (2019).
[9] David Tománek, *Guide Through the Nanocarbon Jungle* (IOP Publishing, Bristol, UK, 2014), p. 2053.
[10] A. G. Rinzler, J. Liu, H. Dai, P. Nikolaev, C. B. Huffman, F. J. Rodríguez-Macías, P. J. Boul, A. H. Lu, D. Heymann, D. T. Colbert, R. S. Lee, J. E. Fischer, A. M. Rao, P. C. Eklund, and R. E. Smalley, Large-scale purification of single-wall carbon nanotubes: Process, product, and characterization, Appl. Phys. A **67**, 29 (1998).
[11] L. J. Sweetman, L. Nghiem, I. Chironi, G. Triani, M. in het Panhuis, and S. F. Ralph, Synthesis, properties and water permeability of SWNT buckypapers, J. Mater. Chem. **22**, 13800 (2012).
[12] Md Harun-Or Rashid, Son Q. T. Pham, Luke J. Sweetman, Leighton J. Alcock, Anthony Wise, Long D. Nghiem, Gerry Triani, Marc in het Panhuis, and Stephen F. Ralph, Synthesis, properties, water and solute permeability of MWNT buckypapers, J. Memb. Sci. **456**, 175 (2014).
[13] Mei Zhang, Ken R. Atkinson, and Ray H. Baughman, Multifunctional carbon nanotube yarns by downsizing an ancient technology, Science **306**, 1358 (2004).
[14] Xiaogang Luo, Wei Weng, Yunxia Liang, Zexu Hu, Yang Zhang, Junjie Yang, Lijun Yang, Shengyuan Yang, Meifang Zhu, and Hui-Ming Cheng, Multifunctional fabrics of carbon nanotube fibers, J. Mater. Chem. A **7**, 8790 (2019).
[15] Md Harun-Or Rashid and Stephen F. Ralph, Carbon nanotube membranes: Synthesis, properties, and future filtration applications, Nanomaterials **7**, 99 (2017).

[16] K. C. Ho, Y. H. Teow, A. W. Mohammad, W. L. Ang, and P. H. Lee, Development of graphene oxide (GO)/multi-walled carbon nanotubes (MWCNTs) nanocomposite conductive membranes for electrically enhanced fouling mitigation, J. Memb. Sci. **552**, 189 (2018).

[17] Rodolfo E. Pérez-Roa, Marc A. Anderson, Dan Rittschof, Christopher G. Hunt, and Daniel R. Noguera, Involvement of reactive oxygen species in the electrochemical inhibition of barnacle (*Amphibalanus amphitrite*) settlement, Biofouling **25**, 563 (2009).

[18] Jae Hyun Park, Susan B. Sinnott, and N. R. Aluru, Ion separation using a Y-junction carbon nanotube, Nanotechnology **17**, 895 (2006).

[19] H. P. Boehm, A. Clauss, and U. Hofmann, Graphite oxide and its membrane properties, J. Chim. Phys. **58**, 141 (1961).

[20] Meng Hu, Sunxiang Zheng, and Baoxia Mi, Organic fouling of graphene oxide membranes and its implications for membrane fouling control in engineered osmosis, Environ. Sci. Technol. **50**, 685 (2016).

[21] William S. Hummers and Richard E. Offeman, Preparation of graphitic oxide, J. Am. Chem. Soc. **80**, 1339 (1958).

[22] Benjamin Collins Brodie, XIII. On the atomic weight of graphite, Phil. Trans. Roy. Soc. (London) **149**, 249 (1859).

[23] Omid Akhavan and Elham Ghaderi, Toxicity of graphene and graphene oxide nanowalls against bacteria, ACS Nano **4**, 5731 (2010).

[24] Inhwa Jung, Daniel A. Field, Nicholas J. Clark, Yanwu Zhu, Dongxing Yang, Richard D. Piner, Sasha Stankovich, Dmitriy A. Dikin, Heike Geisler, Carl A. Ventrice, and Rodney S. Ruoff, Reduction kinetics of graphene oxide determined by electrical transport measurements and temperature programmed desorption, J. Phys. Chem. C **113**, 18480 (2009).

[25] Abozar Akbari, Phillip Sheath, Samuel T. Martin, Dhanraj B. Shinde, Mahdokht Shaibani, Parama Chakraborty Banerjee, Rachel Tkacz, Dibakar Bhattacharyya, and Mainak Majumder, Large-area graphene-based nanofiltration membranes by shear alignment of discotic nematic liquid crystals of graphene oxide, Nat. Commun. **7**, 10891 (2016).

[26] Giancarlo Cicero, Jeffrey C. Grossman, Eric Schwegler, Francois Gygi, and Giulia Galli, Water confined in nanotubes and between graphene sheets: A first principle study, J. Am. Chem. Soc. **130**, 1871 (2008).

[27] Mikhail V. Korobov, Aleksandr V. Talyzin, Anastasiya T. Rebrikova, Elizaveta A. Shilayeva, Natalya V. Avramenko, Alexander N. Gagarin, and Nikolay B. Ferapontov, Sorption of polar organic solvents and water by graphite oxide: Thermodynamic approach, Carbon **102**, 297 (2016).

[28] Abhijit Gogoi, Tukhar Jyoti Konch, Kalyan Raidongia, and K. Anki Reddy, Water and salt dynamics in multilayer graphene oxide (GO) membrane: Role of lateral sheet dimensions, J. Membrane Sci. **563**, 785 (2018).

[29] A. Lerf, A. Buchsteiner, J. Pieper, S. Schöttl, I. Dekany, T. Szabo, and H. P. Boehm, Hydration behavior and dynamics of water molecules in graphite oxide, J. Phys. Chem. Solids **67**, 1106 (2006).

[30] Haiwei Dai, Zhijun Xu, and Xiaoning Yang, Water permeation and ion rejection in layer-by-layer stacked graphene oxide nanochannels: A molecular dynamics simulation, J. Phys. Chem. C **120**, 22585 (2016).

[31] Alexandra Buchsteiner, Anton Lerf, and Jörg Pieper, Water dynamics in graphite oxide investigated with neutron scattering, J. Phys. Chem. B **110**, 22328 (2006).

[32] William L. Jorgensen, Jayaraman Chandrasekhar, Jeffry D. Madura, Roger W. Impey, and Michael L. Klein, Comparison of simple potential functions for simulating liquid water, J. Chem. Phys. **79**, 926 (1983).

[33] A. G. Volkov, S. Paula, and D. W. Deamer, Two mechanisms of permeation of small neutral molecules and hydrated ions across phospholipid bilayers, Bioelectrochem. Bioenerg. **42**, 153 (1997).

[34] R. Mancinelli, A. Botti, F. Bruni, M. A. Ricci, and A. K. Soper, Hydration of sodium, potassium, and chloride ions in solution and the concept of structure maker/breaker, J. Phys. Chem. B **111**, 13570 (2007).

[35] Arindam Bankura, Vincenzo Carnevale, and Michael L. Klein, Hydration structure of salt solutions from ab initio molecular dynamics, J. Chem. Phys. **138**, 014501 (2013).

[36] M. Meot-Ner (Mautner) and S. G. Lias, *Chemistry Web Book: Thermochemistry of cluster ion data*, NIST Standard Reference Database (SRD) 69 (National Institute of Standards and Technology, Gaithersburg, MD, USA, 2018).

[37] Xiao Feng Pang, *Water: Molecular Structure and Properties* (World Scientific, Singapore, 2014).

[38] Ryan C. Rollings, Aaron T. Kuan, and Jene A. Golovchenko, Ion selectivity of graphene nanopores, Nat. Commun. **7**, 11408 (2016).

[39] Johan Mähler and Ingmar Persson, A study of the hydration of the alkali metal ions in aqueous solution, Inorg. Chem. **51**, 425 (2012).

[40] R. M. Rachman, N. Ghaffour, F. Wali, and G. L. Amy, Assessment of silt density index (SDI) as fouling propensity parameter in reverse osmosis (RO) desalination systems, Desal. Water Treat. **51**, 1091 (2013).

[41] Jiguo Zhang, Zhiwei Xu, Mingjing Shan, Baoming Zhou, Yinglin Li, Baodong Li, Jiarong Niu, and Xiaoming Qian, Synergetic effects of oxidized carbon nanotubes and graphene oxide on fouling control and anti-fouling mechanism of polyvinylidene fluoride ultrafiltration membranes, J. Memb. Sci. **448**, 81 (2013).

[42] Emilio Artacho, E. Anglada, O. Dieguez, J. D. Gale, A. Garcia, J. Junquera, R. M. Martin, P. Ordejon, J. M. Pruneda, D. Sanchez-Portal, and J. M. Soler, The siesta method; developments and applicability, J. Phys. Cond. Mat. **20**, 064208 (2008).

[43] G. Kresse and J. Furthmüller, Efficient iterative schemes for *ab initio* total-energy calculations using a plane-wave basis set, Phys. Rev. B **54**, 11169 (1996).

[44] G. Kresse and D. Joubert, From ultrasoft pseudopotentials to the projector augmented-wave method, Phys. Rev. B **59**, 1758 (1999).

[45] John P. Perdew, Kieron Burke, and Matthias Ernzerhof, Generalized Gradient Approximation Made Simple, Phys. Rev. Lett. **77**, 3865 (1996).

[46] D. M. Ceperley and B. J. Alder, Ground State of the Electron Gas by a Stochastic Method, Phys. Rev. Lett. **45**, 566 (1980).

[47] J. P. Perdew and A. Zunger, Self-interaction correction to density-functional approximations for many-electron systems, Phys. Rev. B **23**, 5048 (1981).

[48] A. Ambrosetti and P. L. Silvestrelli, Adsorption of rare-gas atoms and water on graphite and graphene by van der waals-corrected density functional theory, J. Phys. Chem. C **115**, 3695 (2011).

[49] N. Troullier and José Luís Martins, Efficient pseudopotentials for plane-wave calculations, Phys. Rev. B **43**, 1993 (1991).

[50] Hendrik J. Monkhorst and James D. Pack, Special points for Brillouin-zone integrations, Phys. Rev. B **13**, 5188 (1976).

[51] M. R. Hestenes and E. Stiefel, Methods of conjugate gradients for solving linear systems, J. Res. Natl. Bur. Stand. (U. S.) **49**, 409 (1952).

[52] Mohan Chen, Hsin-Yu Ko, Richard C. Remsing, Marcos F. Calegari Andrade, Biswajit Santra, Zhaoru Sun, Annabella Selloni, Roberto Car, Michael L. Klein, John P. Perdew, and Xifan Wu, *Ab initio* theory and modeling of water, Proc. Natl. Acad. Sci. **114**, 10846 (2017).

[53] Giacomo Miceli, Stefano de Gironcoli, and Alfredo Pasquarello, Isobaric first-principles molecular dynamics of liquid water with nonlocal van der Waals interactions, J. Chem. Phys. **142**, 034501 (2015).

[54] Alex P. Gaiduk, François Gygi, and Giulia Galli, Density and compressibility of liquid water and ice from first-principles simulations with hybrid functionals, J. Phys. Chem. Lett. **6**, 2902 (2015).

[55] Felix Franks, *Water: A Matrix of Life: Edition 2* (Royal Society of Chemistry, Cambridge, 2000).

[56] M. Holz, S. R. Heil, and A. Sacco, Temperature-dependent self-diffusion coefficients of water and six selected molecular liquids for calibration in accurate ^{1}H NMR PFG measurements, Phys. Chem. Chem. Phys. **2**, 4740 (2000).

[57] Michael J. Gillan, Dario Alfè, and Angelos Michaelides, Perspective: How good is DFT for water? J. Chem. Phys. **144**, 130901 (2016).

[58] Mostafa Youssef, Roland J. M. Pellenq, and Bilge Yildiz, Glassy nature of water in an ultraconfining disordered material: The case of calcium-silicate-hydrate, J. Am. Chem. Soc. **133**, 2499 (2011).

[59] Anton Lerf, Heyong He, Michael Forster, and Jacek Klinowski, Structure of graphite oxide revisited, J. Phys. Chem. B **102**, 4477 (1998).

[60] Peter Debye and P. Scherrer, Interferenz an regellos orientierten Teilchen im Röntgenlicht I, Physikal. Zeitschr. **17**, 277 (1916).

[61] Kris Erickson, Rolf Erni, Zonghoon Lee, Nasim Alem, Will Gannett, and Alex Zettl, Determination of the local chemical structure of graphene oxide and reduced graphene oxide, Adv. Mater. **22**, 4467 (2010).

[62] N. N. Avgul and A. V. Kiselev, in *Chemistry and Physics of Carbon*, edited by P. L. Walker, Jr. (Marcel Dekker, New York, 1970), Vol. 6, p. 105.

[63] G. Algara-Siller, O. Lehtinen, F. C. Wang, R. R. Nair, U. Kaiser, H. A. Wu, A. K. Geim, and I. V. Grigorieva, Square ice in graphene nanocapillaries, Nature **519**, 443 (2015).

[64] Wu Zhou, Kuibo Yin, Canhui Wang, Yuyang Zhang, Tao Xu, Albina Borisevich, Litao Sun, Juan Carlos Idrobo, Matthew F. Chisholm, Sokrates T. Pantelides, Robert F. Klie, and Andrew R. Lupini, The observation of square ice in graphene questioned, Nature **528**, E1 (2015).

[65] Danil W. Boukhvalov, Mikhail I. Katsnelson, and Young Woo Son, Origin of anomalous water permeation through graphene oxide membrane, Nano Lett. **13**, 3930 (2013).

[66] Tatsuhiko Ohto, Mayank Dodia, Sho Imoto, and Yuki Nagata, Structure and dynamics of water at the water-air interface using first-principles molecular dynamics simulations within generalized gradient approximation, J. Chem. Theory Comput. **15**, 595 (2019).

[67] R. C. Weast, *CRC Handbook of Chemistry and Physics* (CRC Press, Boca Raton, FL, USA, 1986), 67th ed.

[68] Uri Raviv, Pierre Laurat, and Jacob Klein, Fluidity of water confined to subnanometre films, Nature **413**, 51 (2001).

[69] R. C. Major, J. E. Houston, M. J. McGrath, J. I. Siepmann, and X.-Y. Zhu, Viscous Water Meniscus under Nanoconfinement, Phys. Rev. Lett. **96**, 177803 (2006).

[70] Allen Hunt, Robert Ewing, and Behzad Ghanbarian, Percolation Theory for Flow in Porous Media, Lecture Notes in Physics, Vol. 880 (Springer International Publishing, Cham, ZG, Switzerland, 2014).

[71] See Supplemental Material at http://link.aps.org/supplemental/10.1103/PhysRevApplied.12.024054 for videos of molecular dynamics simulations of water molecules and hydrated ions permeating through an all-carbon membrane, provided free of charge.

[72] Heyong He, Jacek Klinowski, Michael Forster, and Anton Lerf, A new structural model for graphite oxide, Chem. Phys. Lett. **287**, 53 (1998).

[73] A. Bondi, van der Waals volumes and radii, J. Phys. Chem. **68**, 441 (1964).

[74] Robert M. Silverstein, Francis X. Webster, David J. Kiemle, and David L. Bryce, *Spectrometric Identification of Organic Compounds* (John Wiley & Sons, Inc., 2014).

[75] Declan A. Doyle, Declan A. Doyle, Morais Cabral, Richard A. Pfuetzner, Anling Kuo, Jacqueline M. Gulbis, Steven L. Cohen, Brian T. Chait, and Roderick Mackinnon, The structure of the potassium channel: Molecular basis of K^+ conduction and selectivity, Science **280**, 69 (1998).

[76] Yufeng Zhou, João H. Morais-Cabral, Amelia Kaufman, and Roderick MacKinnon, Chemistry of ion coordination and hydration revealed by a K^+ channel–fab complex at 2.0 Å resolution, Nature **414**, 43 (2001).

[77] Biswajit Sadhu, Mahesh Sundararajan, and Tusar Bandyopadhyay, Selectivity of a singly permeating ion in nonselective NaK channel: Combined QM and MD based investigations, J. Phys. Chem. B **119**, 12783 (2015).

[78] Jay R. Werber, Akshay Deshmukh, and Menachem Elimelech, The critical need for increased selectivity, not increased water permeability, for desalination membranes, Environ. Sci. Tech. Let. **3**, 112 (2016).

[79] Luka Pocivavsek, Joseph Pugar, Robert O'Dea, Sang-Ho Ye, William Wagner, Edith Tzeng, Sachin Velankar, and Enrique Cerda, Topography-driven surface renewal, Nature Phys. **14**, 948 (2018).

[80] Noam Lior, Ali El-Nashar, and Corrado Sommariva, in *Advances in Water Desalination* (John Wiley & Sons, Ltd, Hoboken, NJ, USA, 2012), Chap. 6, p. 494.

[81] Yanbing Yang, Xiangdong Yang, Ling Liang, Yuyan Gao, Huanyu Cheng, Xinming Li, Mingchu Zou, Renzhi Ma, Quan Yuan, and Xiangfeng Duan, Large-area graphene-nanomesh/carbon-nanotube hybrid membranes for ionic and molecular nanofiltration, Science **364**, 1057 (2019).